Development of Ti/Au Transition-Edge Sensors for Single-Photon Detection

Development of Ti/Au Transition-Edge Sensors for Single-Photon Detection

Xiaolong Xu, Xiaoying Sun, Jian Chen, Mauro Rajteri, Hobey Garrone, Carlo Pepe, Wan Li, Jinjin Li, Mingyu Zhang, Tianjia Bu, Ying Gao, Tianbao Sun and Xueshen Wang

***Abstract*—Transition-edge sensors (TESs) have shown remarkable energy resolution and photon-number resolving ability. In this paper, we report the fabrication and characterization of Ti/Au optical TESs for the detection of single photon at the telecommunication wavelength 1550 nm. A SiO_2/SiN_x antireflection coating is deposited on top of TESs by an inductively coupled plasma-assisted plasma-enhanced chemical vapor deposition (ICP-PECVD) process to improve the detection efficiency. Ti/Au (50/60 nm) TES with a small sensitive area 10 µm × 10 µm shows an energy resolution of 0.12 eV. The TES with a large sensitive area 20 µm × 20 µm can discriminate up to 55 incident photons and the detection efficiency is 46%.**

***Index Terms*—Ti/Au, Transition-Edge Sensor, antireflection coating, photon-number resolving, detection efficiency.**

I. INTRODUCTION

Transition-edge sensors, thanks to their intrinsic energy resolution, can resolve and count photons number detected in a light pulse of an attenuated diode laser[1]. TESs have been designed for a wide energy range, from gamma-ray[2], X-ray[3], UV-visible[4] to NIR[5] photons.

For the quantum information field [6]–[9], the photon-number resolution is a vital parameter and fast response is required. Optical TESs with small sensitive area and suitable transition temperatures could realize sub-microsecond response, sacrificing the performance of saturation energy. For optical quantum metrology[10]–[12], TESs provide near-unity quantum efficiency with an overall 98% quantum efficiency at 850 nm, which is still the highest record ever reported [13][14]. For the optical quantum computing[15], up to 50 photons per pulse and detection efficiencies of 64% were achieved. For quantum optics[16], expressly for the biological fluorescence application[17], TES achieved 67 meV energy resolution at 1550 nm. The high energy resolution could reduce the error of photon number resolution to 1%, and the emission peak between different fluorescent dye could also be separated. This result is also the highest achievement ever reported[18].

In this paper, we report our achievement on the optical TESs with two types of sensitive areas for the single-photon detection at 1550 nm. An optical SiO_2/SiN_x antireflection coating is designed to improve detection efficiency. The TES with the small sensitive area shows an energy resolution of 0.12 eV and that with the large sensitive area shows a wide dynamic detection range of 55 photons.

Manuscript received 26 September 2023; revised 27 November 2023; accepted 18 December 2023. This research was supported by National Key R&D Program of China (Grant No 2022YFF0608303). (Corresponding author: Jinjin Li and Xueshen Wang.)

Xiaolong Xu, Jian Chen, Wan Li, Jinjin Li, Mingyu Zhang, Tianjia Bu, Ying Gao, Tianbao Sun and Xueshen Wang are with the National Institute of Metrology (NIM), 100029 Beijing, China (e-mail: xiaolong.xu@nim.ac.cn; chenjian@nim.ac.cn; liwan0402@163.com; jinjinli@nim.ac.cn; zhangmy@nim.ac.cn; butj@nim.ac.cn; gaoying2018@nim.ac.cn; suntb@nim.ac.cn; wangxs@nim.ac.cn).

Xiaoying Sun is with School of Information Engineering, Shenyang University of Chemical Technology,110142 Shenyang, China (e-mail: sxy17863904210@163.com)

Mauro Rajteri is with the Istituto Nazionale di Ricerca Metrologica (INRiM), 10135 Torino, Italy (e-mail: m.rajteri@inrim.it).

Hobey Garrone, Carlo Pepe are with Department of Electronics and Telecommunications, Politecnico di Torino, 10129 Turin, Italy (e-mail: hobey.garrone@polito.it; carlo.pepe@polito.it)

Color versions of one or more of the figures in this article are available online at http://ieeexplore.ieee.org

II. FABRICATION OF TI/AU TESS

A. Ti/Au bilayer films

The TESs are based on the Ti/Au bilayer superconducting films fabricated by DC magnetron sputtering technique [19], [20]. The cross section of a Ti/Au film is characterized by a high-resolution transmission electron microscope (HRTEM, Thermo Scientific Talos F200) and shown in Fig. 1. The upper part shows the hexagonal Ti crystal (PDF#44-1294), and the lattice spacing is 2.24Å responding to the (101) orientation. The (111) plane of the cubic Au crystal (PDF#04-0784) with the lattice spacing 2.35 Å is observed in the bottom part.

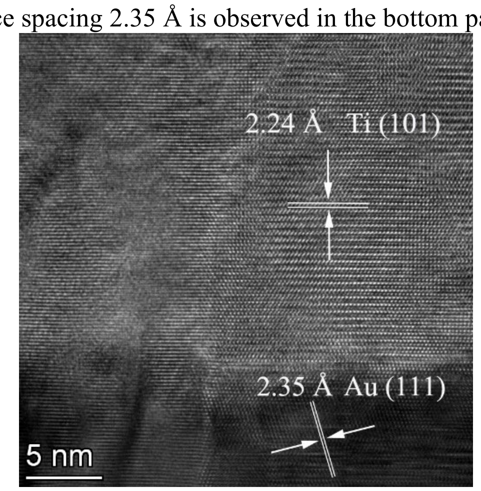

Fig. 1. The HRTEM image of the Ti/Au interface.

B. Ti/Au TESs

The thicknesses of the Ti and Au films, and the two types of effective sensitive areas (A_s) are shown in Table 1. The Ti/Au

A_s, and the Nb superconducting leads are defined with the UV lithography and lift-off processes. The antireflection structure comprised by two dielectric layers SiO_2 and SiN_x is deposited by ICP-PECVD. The optical images of the two types of TES are shown in Fig. 2. Considering the heat capacity, the NIM10 will show a better energy resolution compared to NIM20, already reported in a previous work [20]. The measurements of NIM20 in this work focused on the dynamic range and quantum efficiency.

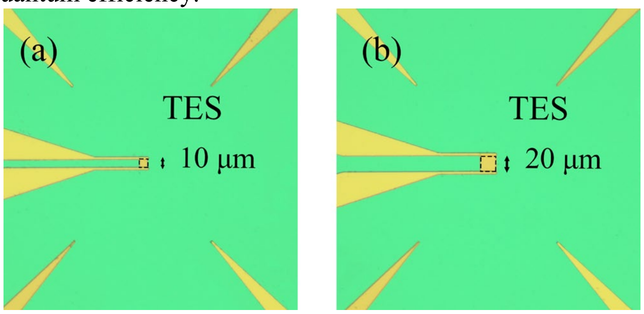

Fig. 2. The optical images of Ti/Au TESs with two types of *As*.

TABLE I
THE PAREMETERS OF TI/AU TESS

Sample	Thickness/nm		T_c /mK	ΔT_c/mK	A_s/μm^2
	Ti	Au			
NIM10	50	60	97.8	4.7	10×10
NIM20	50	60	95.2	4.3	20×20

Fig. 3 shows the simulated and measured reflectivity results of the SiO_2 (490 nm)/SiN_x (200 nm)/Ti (50 nm)/Au (60 nm)/Ti (5 nm)/SiN_x (500 nm)/Si optical structure. The reflectivity is measured with a Horiba UVISEL2 spectroscopic ellipsometer. The minimum values of the initial simulation, corrected simulation and measured reflectivity are 10.5% at 1583 nm, 11.6% at 1533 nm and 11.2% at 1530 nm, respectively. The difference on the wavelength with the lowest reflectivity may be caused by the thicknesses deviation of the optical structure.

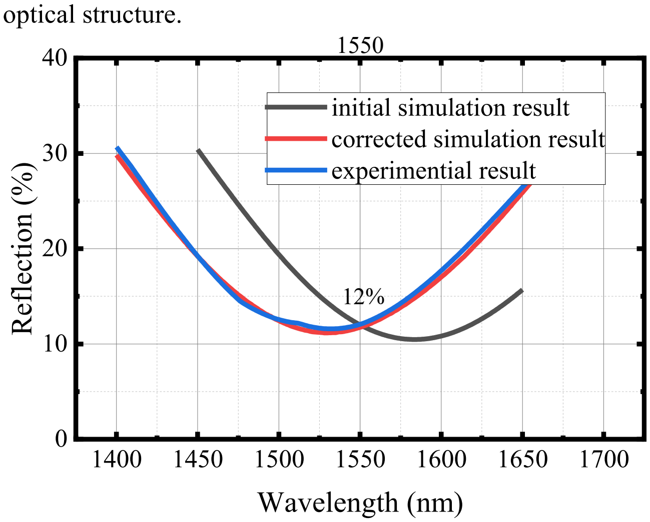

Fig. 3. Simulated and measured reflectivity results of the SiO_2/SiN_x/Ti/Au/Ti/SiN_x/Si optical structure.

The TESs is prepared according to the initial simulation structure, but we found that there is a certain difference between the actual experimental value of the sample and the initial simulation value, so we tried to correct this difference by adjusting the thickness of the films. The thickness of Ti is corrected to +3 nm out of 50 nm, the thickness of SiO_2 is corrected to -4 nm out of 490 nm, and the thickness of SiN_x is corrected to -5 nm out of 200 nm. The measured reflectivity is 12% at 1550 nm.

III. SINGLE PHOTON DETECTION RESULTS

The TESs were characterized in an adiabatic demagnetization refrigerator (ADR) system. The base temperature is 30 mK. An optical fiber is mounted on the TES with UV-resin, and the diameter of the fiber core is 8.2 μm. The pigtail of the optical fiber is connected to an attenuated pulsed diode laser with a wavelength of 1540 nm. The pulse width is 37 ps, and the repetition rate is 1 kHz. The photon number in one pulse is controlled by adjustable attenuation.

A. Pulse response and energy resolution of the small sensitive area TES NIM10

NIM10 is measured with a four-wire method using an ac resistance bridge. 1 μA excitation current is applied. The resistance versus temperature curve is plotted in Fig. 4. The transition temperature is ~ 97.8 mK, and the width of the transition edge ΔT_c is about 4.7 mK. The normal metal resistance R_n is 0.5 Ω.

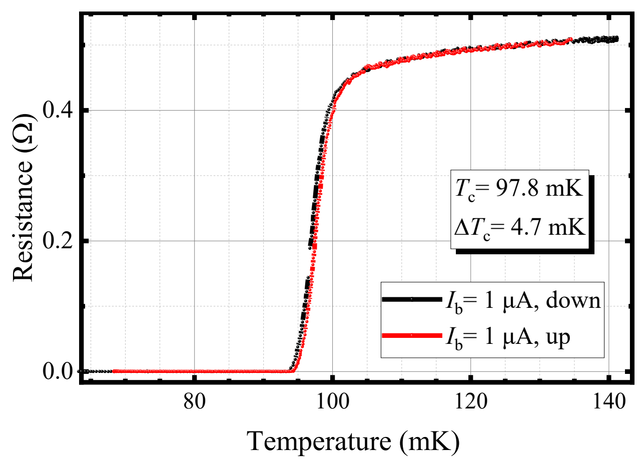

Fig. 4. The Resistance versus temperature curve of NIM10.

The typical single photon pulse response is shown in Fig. 5. the electrical time constant $\tau_{eletrical}$ is 70 ns and the effective time constant τ_{etf} is 63 μs, by fitting the double exponential equation[21].

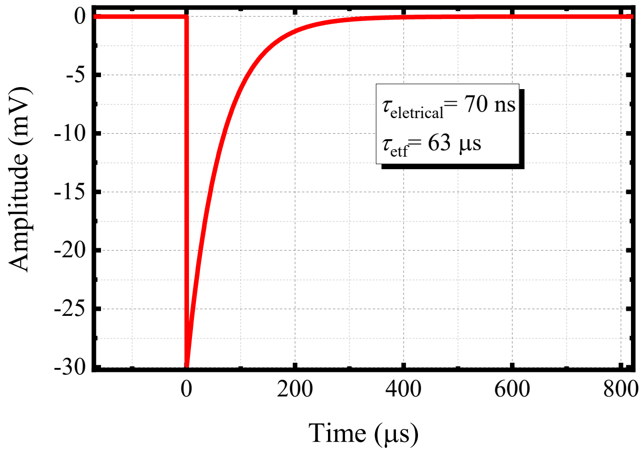

Fig. 5. Typical single photon pulse response of NIM10

The histograms of pulse amplitude are plotted and shown in Fig.6. A low pass filter at 200 kHz is used during the counting. The detected mean photon number μ is 0.6 photons per pulse, and a typical Poisson distribution is shown. The full width at half maximum (FWHM) energy resolution ΔE is 0.12 eV. NIM10 has a lower heat capacity compared to NIM20 of which the energy resolution is 0.19 eV reported in the previous work[20]. Abnormal baseline fluctuations appear between two photon states, which could be due to the misalignment of optical fiber. Due to the offset position, some photons are absorbed by leads or substrate, which generates lower amplitude pulses with respect to the pulse generated by the direct photon absorption on the TES sensitive area.

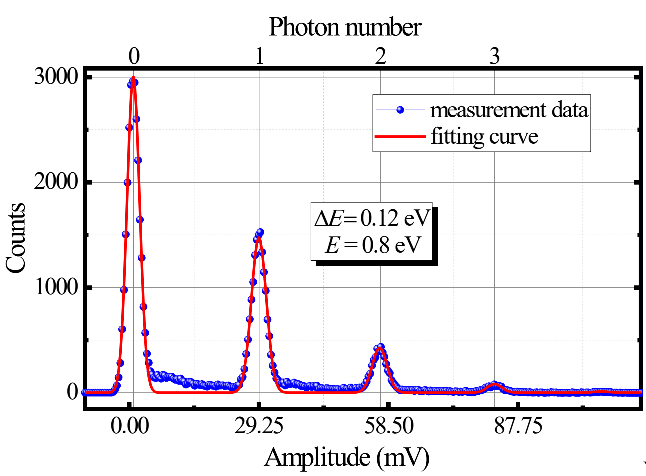

Fig. 6. The amplitude histogram for 4 photons states for NIM10.

B. Dynamic range and detection efficiency of the large sensitive area TES NIM20

The dynamic range of photon counting and the detection efficiency of the large sensitive area TES NIM20 are characterized. Fig. 7 shows the wide dynamic range of photon counting, and up to 55 photons can be discriminated. This data is obtained by changing the optical attenuation during the acquisition. The attenuation gradually decreases from 60 dB to 40 dB. Fig. 7b shows the enlargement of the high photon states counting part of Fig. 7a. Fig. 7b inset shows the response remains linear within 16 photons with the adjusted R-square is 0.99903. For the high photon states, the valleys between the peaks could not fall back to baseline which was also shown in other work[22]. The large sensitive area induces high saturation energy due to the larger heat capacity. This will bring benefits to the evaluation of the attenuation single photon laser source using optical TESs. The wide dynamic range enables TES to have a wider observation window, making it easier for operators to find the correct attenuation factor of the laser source. Moreover, the good linearity benefits the calibration of photons with various energy.

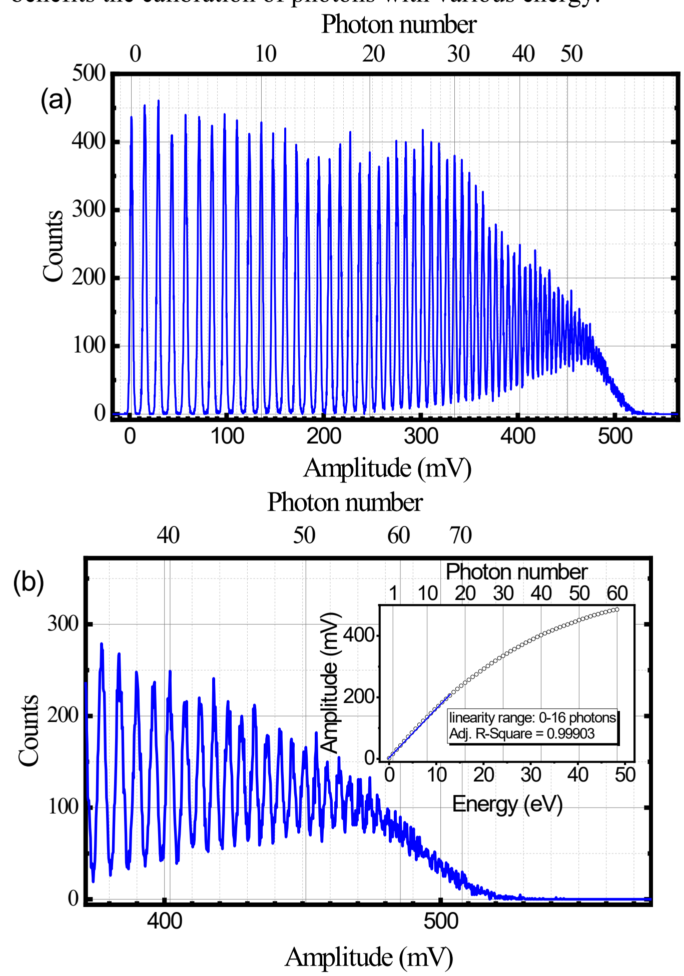

Fig. 7. The photon counting ability of NIM20. (a) the full spectrum of photon counting states, (b) the enlargement of high photon states counting part, the inset is the response linearity *vs*. photon number.

For the detection efficiency measurements, the optical path is firstly connected to the power meter through an adjustable attenuator. A suitable attenuation is set up, and then the optical path is spliced with fiber of NIM20. The detection efficiency is defined as the ratio of the detected mean photons to the input mean photons. Fig. 8 shows the input mean photons vs. detected ones. By fitting the linear results detected mean photon number from TES and the input mean photon evaluated from the power meter, we get the quantum efficiency η to be

46%±0.4%. This is much lower than the intrinsic 88% efficiency which may be caused by the geometric losses during the fiber alignment process.

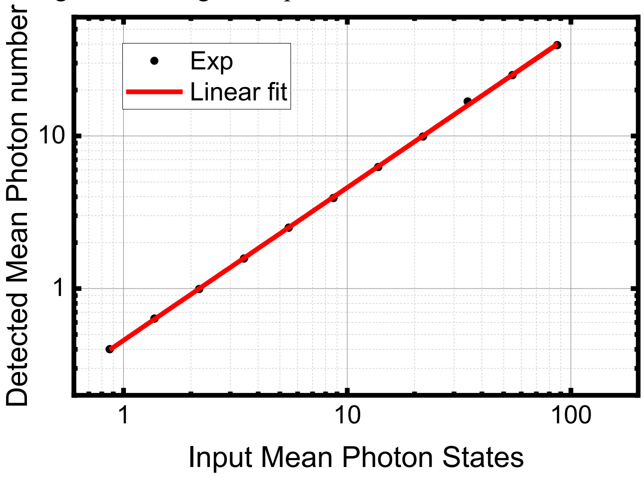

Fig. 8. The detected mean photons vs the input mean photons.

V. Conclusion

The optical Ti/Au TES shows an energy resolution of 0.12 eV with a sensitive area 10 × 10 μm^2. For the TES with a larger sensitive area 20 × 20 μm^2 with a SiN_x/SiO_2 antireflection layer, 55 photon states can be discriminated, and the quantum efficiency is 46%. A small TES is favorable for realizing a high energy resolution ability. In the future, we will develop TESs with high detection efficiency and a more reliable fiber alignment process, in view of their application to optical quantum metrology.

Acknowledgment

The authors would like to thank Mrs. Qing Zhong at NIM for the helpful discussions.

References

[1] A. E. Lita, D. V Reddy, V. B. Verma, R. P. Mirin, and S. W. Nam, "Development of superconducting single-photon and photon-number resolving detectors for quantum applications," *J. Light. Technol.*, vol. XX, no. X, pp. 1–21, 2022.

[2] D. A. Bennett *et al.*, "A high resolution gamma-ray spectrometer based on superconducting microcalorimeters," *Rev. Sci. Instrum.*, vol. 83, no. 9, p. 093113, Sep. 2012.

[3] E. Taralli *et al.*, "AC/DC Characterization of a Ti/Au TES with Au/Bi Absorber for X-ray Detection," *J. Low Temp. Phys.*, vol. 199, no. 1–2, pp. 102–109, 2020.

[4] E. Taralli *et al.*, "Reduced Active Area in Transition-Edge Sensors for Visible-NIR Photon Detection: A Comparison of Experimental Data and Two-Fluid Model," *IEEE Trans. Appl. Supercond.*, vol. 25, no. 3, pp. 1–4, Jun. 2015.

[5] P. Z. Li *et al.*, "Development of Self-aligned Ti Optical Transition-Edge Sensors at 1550 nm," *J. Low Temp. Phys.*, vol. 209, no. 3–4, pp. 248–255, 2022.

[6] R. H. Hadfield, "Single-photon detectors for optical quantum information applications," *Nat. Photonics*, vol. 3, no. 12, pp. 696–705, 2009.

[7] T. Gerrits, A. Lita, B. Calkins, and S. W. Nam, "Superconducting Transition Edge Sensors for Quantum Optics," 2016, pp. 31–60.

[8] F. E. Becerra, J. Fan, and A. Migdall, "Photon number resolution enables quantum receiver for realistic coherent optical communications," *Nat. Photonics*, vol. 9, no. 1, pp. 48–53, Jan. 2015.

[9] K. Tsujino *et al.*, "Quantum Receiver beyond the Standard Quantum Limit of Coherent Optical Communication," *Phys. Rev. Lett.*, vol. 106, no. 25, p. 250503, Jun. 2011.

[10] J. C. F. Matthews *et al.*, "Towards practical quantum metrology with photon counting," *npj Quantum Inf.*, vol. 2, no. 1, 2016.

[11] M. von Helversen *et al.*, "Quantum metrology of solid-state single-photon sources using photon-number-resolving detectors," *New J. Phys.*, vol. 21, no. 3, p. 035007, Mar. 2019.

[12] V. Giovannetti, S. Lloyd, and L. Maccone, "Quantum Metrology," *Phys. Rev. Lett.*, vol. 96, no. 1, p. 010401, Jan. 2006.

[13] D. Fukuda *et al.*, "Titanium-based transition-edge photon number resolving detector with 98% detection efficiency with index-matched small-gap fiber coupling," *Opt. Express*, vol. 19, no. 2, p. 870, Jan. 2011.

[14] A. E. Lita, A. J. Miller, and S. W. Nam, "Counting near-infrared single-photons with 95% efficiency," *Opt. Express*, vol. 16, no. 5, p. 3032, 2008.

[15] G. Harder, T. J. Bartley, A. E. Lita, S. W. Nam, T. Gerrits, and C. Silberhorn, "Single-Mode Parametric-Down-Conversion States with 50 Photons as a Source for Mesoscopic Quantum Optics," *Phys. Rev. Lett.*, vol. 116, no. 14, p. 143601, Apr. 2016.

[16] D. Fukuda, K. Niwa, K. Hattori, S. Inoue, R. Kobayashi, and T. Numata, "Confocal Microscopy Imaging with an Optical Transition Edge Sensor," *J. Low Temp. Phys.*, vol. 193, no. 5–6, pp. 1228–1235, Dec. 2018.

[17] D. FUKUDA, "Single-Photon Measurement Techniques with a Superconducting Transition Edge Sensor," *IEICE Trans. Electron.*, vol. E102.C, no. 3, pp. 230–234, Mar. 2019.

[18] K. Hattori, T. Konno, Y. Miura, S. Takasu, and D. Fukuda, "An optical transition-edge sensor with high energy resolution," *Supercond. Sci. Technol.*, vol. 35, no. 9, p. 095002, Sep. 2022.

[19] X. Xu *et al.*, "Investigation of Superconducting Ti/Ti-Au/Au Tri-Layer Films With a Co-Sputtering Process for Transition-Edge Sensors," *IEEE Trans. Appl. Supercond.*, vol. 33, no. 5, pp. 1–5, Aug. 2023.

[20] X. Xu *et al.*, "Investigation of Ti/Au Transition-Edge Sensors for Single-Photon Detection," *J. Low Temp. Phys.*, vol. 209, no. 3–4, pp. 372–378, Nov. 2022.

[21] L. Lolli, E. Taralli, M. Rajteri, T. Numata, and D. Fukuda, "Characterization of Optical Fast Transition-Edge Sensors With Optimized Fiber Coupling," *IEEE Trans. Appl. Supercond.*, vol. 23, no. 3, pp. 2100904–2100904, Jun. 2013.

[22] L. Lolli, E. Taralli, and M. Rajteri, "Ti/Au TES to Discriminate Single Photons," *J. Low Temp. Phys.*, vol. 167, no. 5–6, pp. 803–808, Jun. 2012.